

A semi-automatic algorithm for grey level estimation in tomography

K.J. Batenburg^{a,b}, W. van Aarle^b, J. Sijbers^b

^a*Centrum Wiskunde en Informatica
Science Park 123, NL-1098XG, Amsterdam, The Netherlands*
^b*IBBT-Vision Lab, University of Antwerp
Universiteitsplein 1, B-2610, Wilrijk, Belgium*

Abstract

Discrete tomography is a powerful approach for reconstructing images that contain only a few grey levels from their projections. Most theory and reconstruction algorithms for discrete tomography assume that the values of these grey levels are known in advance. In many practical applications, however, the grey levels are unknown and difficult to estimate. In this paper, we propose a semi-automatic approach for grey level estimation that can be used as a preprocessing step before applying discrete tomography algorithms. We present experimental results on its accuracy in simulation experiments.

Keywords: Discrete tomography, grey level estimation, segmentation.

1. Introduction

The field of *tomography* deals with the reconstruction of images (known as *tomograms*) from their projections, taken along a range of angles. Tomography has a wide range of applications in medicine, industry, and science. According to Herman and Kuba [1, 2], the field of *discrete tomography* is concerned with the reconstruction of images from a small number of projections, where the set of pixel values is known to have only a few discrete values. It must be noted that the term “*discrete*” is often used to indicate the *discrete domain* of the image, i.e., when reconstructing lattice sets. In this paper, we adhere to the former definition, and focus on the reconstruction of images that consist of a

small number of grey levels from their (non-lattice) X-ray projections.

A variety of reconstruction algorithms have been proposed for discrete tomography problems. In Schüle et al. [3], an algorithm is presented for reconstructing binary images from a small number of projections. This primal-dual subgradient algorithm is applied to a suitable decomposition of the objective functional, yielding provable convergence to a binary solution. In Batenburg [4], a similar reconstruction problem is modeled as a series of network flow problems in graphs, that are solved iteratively. Both Liao and Herman [5] and Alpers et al. [6] consider reconstruction problems that may involve more than two grey levels, employing statistical models based on Gibbs priors for their solution. The iterative *DART* algorithm was recently proposed as an efficient heuristic reconstruction algorithm for large-scale discrete tomography problems Batenburg and Sijbers [7], Batenburg et al. [8]. It has been applied successfully to a range of experimental electron tomography datasets, leading to various new insights in the structure of nanomaterials (Bals et al. [9, 10]).

Besides the assumption on the grey levels, many of these algorithms incorporate additional prior knowledge of the original object that needs to be reconstructed. A preference for locally smooth regions is typically incorporated, as it corresponds to a range of practical images. By combining such prior knowledge with knowledge of the grey levels, it is often possible to compute accurate reconstructions from just a small number of projections. In some cases, as few as three projections are already sufficient to compute a high-quality reconstruction.

A common assumption in all these reconstruction algorithms, is that the set of admissible grey levels is known *a priori*. Although this assumption is easy to satisfy in simulation experiments, obtaining prior knowledge of the set of possible grey levels is often not straightforward in practical applications, for several reasons:

- Even when the number of materials that constitute the scanned object is known, the densities of these materials may be unknown.
- When the materials and their densities *are* known in advance, calibra-

tion is required to translate the material properties into a reconstructed grey level. The calibration parameters depend not only on the scanned materials, but also on various properties of the scanner system. In many experimental settings, such information is not available.

- Calibration parameters of the scanning system may change over time. For example, the X-ray source of a micro-CT scanner heats up while scanning, changing the spectrum of emitted X-rays. While this may have a negligible effect on the calibration parameters during a single scan, batch processing of scans may change the parameters, and consequently change the grey levels in the reconstruction.

When several similar objects are scanned as a single batch, it may be possible to obtain a high quality reconstruction of one of those objects, based on a large number of projections. This reconstruction can then be used to estimate the admissible grey levels for the remaining objects, which can then be reconstructed from few projections. However, many important applications of discrete tomography deal with acquisition systems where it is not possible at all to obtain an accurate reconstruction by conventional, non-discrete reconstruction algorithms. In Materials Science, for example, discrete tomography is used to reconstruct 3D images of nanomaterials from a series of projection images acquired by an electron microscope (Batenburg et al. [8]). Due to the structure of the sample holder, projections can only be obtained for a limited range of angles, resulting in severe reconstruction artifacts for conventional algorithms.

Even in such cases, it may still be possible for an expert user to delineate certain areas in the reconstruction that are likely to have a constant composition in the original object. In this paper, we therefore consider a simpler version of the grey level estimation problem, where the user first selects an image region that can be expected to correspond to a homogenous region in the original object, based on an initial grey-level reconstruction. This initial reconstruction can be obtained by classical, non-discrete reconstruction algorithms. In certain cases, knowledge of such a constant region allows for reliable estimation of the

grey level corresponding to the selected region.

The outline of this paper is as follows. In Section 2, the problem of grey level estimation is introduced, along with formal notation. In Section 3, we present a semi-automatic approach for estimating the grey levels when for each grey level a subset of corresponding pixels is given. Experimental results for a range of simulation experiments are described in Section 4. Section 5 discusses the possibilities for obtaining more accurate estimates, compared to the approach of this paper. Section 6 concludes the paper.

2. Problem and model

The unknown physical object from which projection data has been acquired is represented by a grey value image $f : \mathbb{R}^2 \rightarrow \mathbb{R}$. We denote the set of all such functions f that are measurable and have bounded support by \mathcal{F} , also called the set of *images*.

Projections are measured along lines $l_{\theta,t} = \{(x,y) \in \mathbb{R}^2 : x \cos \theta + y \sin \theta = t\}$, where θ represents the angle between the line and the y -axis and t represents the coordinate along the projection axis; see Fig. 1.

Denote the set of all functions $s : \mathbb{R} \times [0, 2\pi) \rightarrow \mathbb{R}$ by \mathcal{S} . The *Radon transform* $\mathcal{F} \rightarrow \mathcal{S}$ is defined by

$$R(f)(t, \theta) = \iint_{-\infty}^{\infty} f(x, y) \delta(x \cos \theta + y \sin \theta - t) dx dy.$$

with $\delta(\cdot)$ denoting the Dirac delta function. The function $R(f) \in \mathcal{S}$ is also called the *sinogram* of f .

2.1. Grey level estimation problem

The *reconstruction problem* in tomography concerns the recovery of a function f from its Radon transform $R(f)$. Here, we focus on a restriction of f to functions for which the set of grey levels is a small, discrete set $G = \{g_1, \dots, g_k\}$. We denote the set of all such images $f : \mathbb{R}^2 \rightarrow G$ by \mathcal{G} . The main problem of

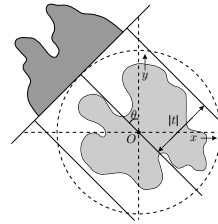


Figure 1: Basic setting of transmission tomography.

this paper consists of estimating the grey levels G from given projection data along a finite set of angles. It is clear that this problem does not have a unique solution in general. A first requirement for a grey level to be recoverable is that it occurs in f as a subset of \mathbb{R}^2 of measure greater than 0. Also, when a small number of projections is available and k is large, it is straightforward to find examples where the grey values cannot be determined uniquely. In this paper, we therefore assume that additional prior knowledge is available, prescribing for each grey level $i = 1, \dots, k$ a region $A_i \subset \mathbb{R}^2$ on which the image is known to have a constant grey level. This prior knowledge is obtained by computing an initial greylevel reconstruction, using a standard tomography algorithm, and let an expert user select regions in this reconstruction that are likely to be constant in the original scanned object.

However, even specifying an entire region where the image is known to be constant is not sufficient to guarantee that the grey levels are uniquely determined by the projection data. In particular, this problem occurs when the number of projections is small. Fig. 2 shows a well-known procedure to generate a so-called *switching component*: a non-zero image that has a zero projection in a given set of projection angles. The procedure is described in Herman and Kuba [1] (Section 4.3, p. 88), where it is used to generate a switching component in the context of lattice sets. For each new direction, a negated copy of the switching component is added, that is translated in the given direction. As shown in Fig. 2, the same procedure applies to images defined on \mathbb{R}^2 , and can also be used to create switching components that are constant, and non-zero, on a given region. The figure shows the subsequent addition of switching components in the horizontal, vertical, and diagonal direction, respectively. A similar construction can be applied for any finite set of projection directions.

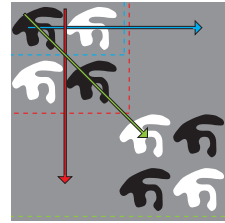


Figure 2: Example of a switching component for three directions, which is constant and nonzero on each of the black and white regions.

Proposition 1. *Let $D = \{\theta_1, \dots, \theta_d\}$ be a given set of projection angles. Let $G = \{g_1, \dots, g_k\}$, $A \subset \mathbb{R}^2$ and $g \in G$. Let $f \in \mathcal{G}$ such that $f(x, y) = g$ for all $(x, y) \in A$. Then for each grey level $\tilde{g} \in \mathbb{R}$, there is an image $\tilde{f} \in \mathcal{F}$ such that $\tilde{f}(x, y) = \tilde{g}$ for all $(x, y) \in A$ and $R(f)(t, \theta_i) = R(\tilde{f})(t, \theta_i)$ for $i = 1, \dots, d$, $t \in \mathbb{R}$. Moreover, there is such an image \tilde{f} that has at most $3k$ grey levels.*

Proof. (sketch) By the construction depicted in Fig. 2, an image can be created that has a constant value of 1 on A , has constant zero projections in all given directions and only contains grey levels from $\{-1, 0, 1\}$. Let $\rho = \tilde{g} - g$. By adding a multiple of ρ times the switching component to f , an image \tilde{f} that conforms to the proposition can be created. This image will have at most $3k$ grey levels, included in the set $\{g_1 - \rho, g_1, g_1 + \rho, g_2 - \rho, g_2, g_2 + \rho, \dots, g_k - \rho, g_k, g_k + \rho\}$. Note that some of these grey levels may be negative, even if the image f has only nonnegative grey levels. \square

2.2. Discretization

In practice, a projection is measured at a finite set of detector cells, each measuring the integral of the object density along a line. Let m denote the total number of measured detector values (for all angles) and let $\mathbf{p} \in \mathbb{R}^m$ denote the measured projection data. We now discretize the images $f \in \mathcal{F}$ as well, represented on a square grid of width w . Let $n = w^2$, the number of pixels in the image. We assume that the image is zero outside this rectangle. Let $\mathbf{v} \in \mathbb{R}^n$ denote the discretized image of the object. The Radon transform for a finite set of angles can now be modeled as a linear operator \mathbf{W} , called the *projection operator*, that maps the image \mathbf{v} to the projection data \mathbf{p} :

$$\mathbf{W}\mathbf{v} = \mathbf{p}. \quad (1)$$

We represent \mathbf{W} by an $m \times n$ matrix $\mathbf{W} = (w_{ij})$. The vector \mathbf{p} is called the *forward projection* or *sinogram* of \mathbf{v} .

The notation introduced above allows us to define the key problem of this paper:

Problem 1. Let $\mathbf{v} \in \mathbb{R}^n$ be an unknown image and let $g \in \mathbb{R}$ be an unknown grey level. Suppose that $\mathbf{p} = \mathbf{W}\mathbf{v}$ is given, and that a set $A \subset \{1, \dots, n\}$ is given such that $v_i = g$ for all $i \in A$. Find g .

2.3. Grey level penalty function

Let $A \subset \{1, \dots, n\}$ and $g \in \mathbb{R}$, as in Problem 1. Reorder the pixels $\{1, \dots, n\}$ and the corresponding columns of \mathbf{W} , such that

$$\mathbf{W} = \left(\mathbf{W}_A \mathbf{W}_B \right), \quad (2)$$

where \mathbf{W}_A contains the columns of \mathbf{W} corresponding to the pixels in A . We then have

$$\mathbf{W}\mathbf{x} = \left(\mathbf{W}_A \mathbf{W}_B \right) \begin{pmatrix} \mathbf{g} \\ \mathbf{v}_B \end{pmatrix} = \mathbf{p}, \quad (3)$$

where \mathbf{g} denotes a constant vector for which all entries are g . This leads to

$$\mathbf{W}_B \mathbf{v}_B = \mathbf{p} - \mathbf{W}_A \mathbf{g}, \quad (4)$$

which provides a necessary condition for a grey level estimate to be correct: Eq. (4) must have a solution. Clearly, this condition is not always sufficient, as emphasized by Prop. 1. Yet, if $|A|$ is a relatively large fraction of n , it can be expected that the condition is also sufficient, at least in many cases. Note that in practice, it may not be possible to solve Eq. (4) exactly, due to noise and discretization errors. Given A , one can measure the inconsistency of a grey level \tilde{g} with the projection data \mathbf{p} using the following *grey level penalty function*

$$P(\tilde{g}) = \min_{\mathbf{v}_B} \|\mathbf{p} - \mathbf{W}_A \tilde{\mathbf{g}} - \mathbf{W}_B \mathbf{v}_B\|, \quad (5)$$

where $\|\cdot\|$ denotes a certain norm, to be defined below.

Note that for each grey level \tilde{g} , there may be multiple vectors \mathbf{v}_B for which the minimum penalty is attained. This does not have to be a problem for grey level estimation, as long as the grey level for which the penalty is minimal is uniquely determined by the projection data. According to Prop. 1, it may occur that the grey level cannot be determined uniquely, in which case we seek to find at least one of the grey levels for which the penalty is minimal.

To minimize the grey level penalty, the penalty function must typically be evaluated in several points. A range of iterative methods are available for solving the minimization problem in Eq. (5). In this paper, we use the SIRT algorithm; see Gilbert [11], Gregor and Benson [12]. Let $\mathbf{v}^{(0)} = \mathbf{0}$. For $q = 1, 2, \dots$, let $\mathbf{r}^{(q)} = \mathbf{p} - \mathbf{W}\mathbf{v}^{(q-1)}$. In each iteration q , the current reconstruction $\mathbf{v}^{(q-1)}$ is updated, yielding a new reconstruction $\mathbf{v}^{(q)}$, as follows:

$$v_j^{(q)} = v_j^{(q-1)} + \frac{1}{\sum_{i=1}^n w_{ij}} \sum_{i=1}^m \frac{w_{ij} r_i^{(q)}}{\sum_{j=1}^m w_{ij}}. \quad (6)$$

The SIRT algorithm converges to a solution of Eq. (5) where the norm to be minimized is a weighted sum of squares Gregor and Benson [12]. To be more precise, let $R = (r_{ij}) \in \mathbb{R}^{m \times m}$ be a diagonal matrix with $r_{ii} = 1/\sum_{j=1}^n w_{ij}$. Then SIRT minimizes the norm $\|\mathbf{W}\mathbf{v} - \mathbf{p}\|_R = (\mathbf{W}\mathbf{v} - \mathbf{p})^T R (\mathbf{W}\mathbf{v} - \mathbf{p})$.

An important physical constraint in most tomography problems, is that the attenuation coefficients of the scanned materials, corresponding to the grey levels in the reconstructed image, cannot be negative. Therefore, it seems that solving Eq. (5) for *nonnegative* \mathbf{v}_B would yield a more powerful penalty function for such cases. However, this problem typically requires significantly more computation effort compared to the unconstrained variant (depending on the norm). As an alternative, we use a heuristic adaptation of the SIRT algorithm, where nonnegative entries of \mathbf{v}_B are set to 0 after each iteration. This approach was already suggested in Gilbert [11], and often results in more accurate reconstructions than the unconstrained version. We denote this version of SIRT by *SIRT-P*.

3. Estimation approach

In this section, we propose the *Discrete Grey Level Selection* approach (DGLS) for estimating grey levels from projection data. Fig. 3 shows a schematic overview of the steps involved in estimating one or more grey levels. The first part of the procedure requires user interaction. Based on an initial reconstruction, obtained by a conventional (i.e., non-discrete) reconstruction algorithm, the user selects

a region, the *user-selected part* (USP), which is expected to belong to a single grey level in the ground truth image, i.e., it should be constant. Note that this region does *not* have to be constant in the initial grey level reconstruction. The user, who typically has substantial implicit prior knowledge of the particular object under investigation, is responsible for selecting a proper region. In this phase, a significant amount of implicit prior knowledge can be input by the user. For example, if the object is known to contain no holes, it will be safe to select a USP that is clearly within the interior of the object. It can be difficult to select a proper region if the number of projections is small. The selected region should not be too small, but should certainly not contain any pixels that correspond to a different grey level. If the original image contains several grey levels, a region must be selected for each grey level that needs to be estimated. The regions A_i , along with the projection data, now form the input of the estimation algorithm.

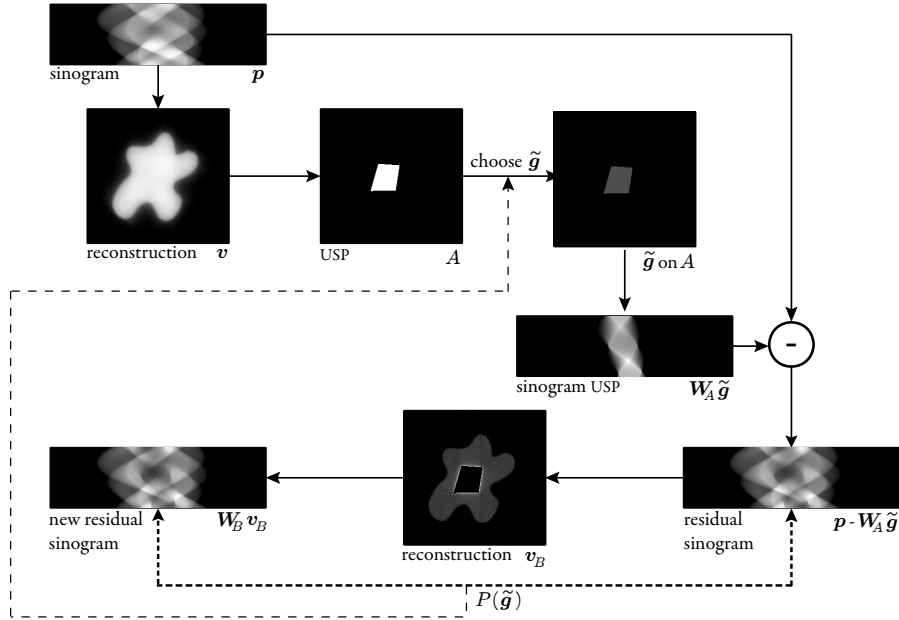


Figure 3: Schematic overview of the Discrete Grey Level Selection procedure.

After selecting the USP of a single grey level, an optimization algorithm is used to minimize the grey level penalty function. To evaluate the penalty func-

tion for a given grey level g , the sinogram $\mathbf{W}_A \mathbf{g}$ of the USP is first subtracted from the complete sinogram \mathbf{p} , forming the right-hand side of Eq. (4). Subsequently, inconsistency of the remaining part of the image with the remaining projection data is determined by evaluating the penalty function (e.g., using SIRT or SIRT-P). Based on the value of the penalty function, the grey level estimate is updated iteratively, until the penalty function is minimized. Evaluating the grey level penalty function can be computationally expensive. To find the minimum of this function using a small number of evaluations, Brent’s method is used, as described in Chapter 5 of Brent [13]. Note that for the SIRT-variant of DGLS, the minimization problem to be solved corresponds to Eq. (5) and is in fact a quadratic problem in the unknown grey level g and the unknown image v_B . In this case, solving for both g and v_B in a combined optimization algorithm, that exploits this structure, can yield the same results in much less computation time. Here, we opted for Brent’s method, as it can be used without changes for both the SIRT and SIRT-P variants of DGLS and it can be easily extended to incorporate other reconstruction algorithms, even if their implementation is considered a black box.

The proposed algorithm estimates a single grey level at a time. If there are multiple grey levels, the USPs for each grey level are selected based on the same initial reconstruction, and the grey level estimations are performed independently for each grey level. A combined approach, that maintains a constant USP for each grey level simultaneously, could also be used. However, this would lead to errors in all estimated grey levels if just one of the USPs is not properly selected. For the experiments in this paper, we therefore focus on independent estimation, as it is likely to be more robust in practice.

4. Experiments and results

4.1. Grey level estimation

Simulation experiments were performed based on four 256×256 phantom images: two binary images (Fig. 4a and b), one image with 3 grey levels (Fig. 4c)

and one with 7 grey levels (Fig. 4d). Additional simulation were performed for a phantom family of 100 phantom images of size 256×256 (four are depicted in Fig. 4e). These images each contain between 3 and 12 ellipses, randomly generated with radii between 10 and 50; for 20% of the ellipses, the value of the corresponding pixels are set to zero, which allows for the creation of gaps inside ellipses already present.

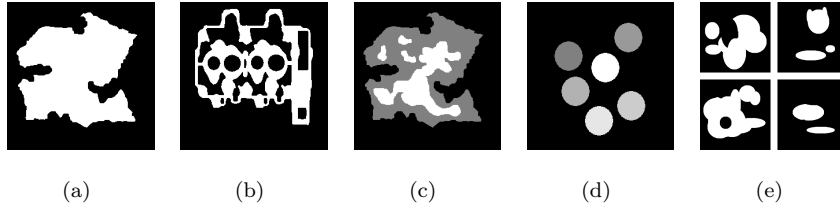
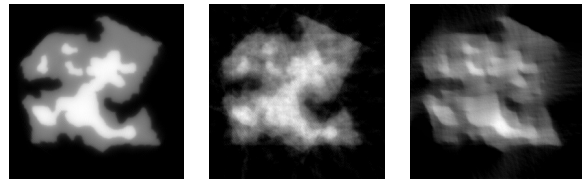


Figure 4: Phantom images used for our simulation experiments.

From each phantom image, a parallel beam sinogram was computed with a varying number of projections, angular range, or noise level. The spacing between projected parallel lines equals the pixel size of the phantom image. Next, the phantom image was reconstructed using both the SIRT and SIRT-P algorithm. Finally, the grey levels of the reconstructed phantom were estimated, either with a simple median value (MED) of the pixels of the user-selected part on the initial reconstruction or with the proposed DGLS approach based on the same USP, using either SIRT or SIRT-P to compute the grey level penalty. For all images, the grey level of the background was assumed to be zero and was therefore not estimated.



(a) 180 angles, 180° range (b) 15 angles, 180° range (c) 30 angles, 100° range

Figure 5: SIRT reconstructions of phantom image 4(c)

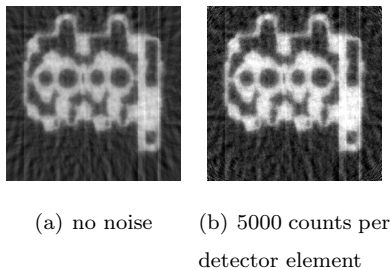


Figure 6: SIRT reconstructions of phantom image 4(b)

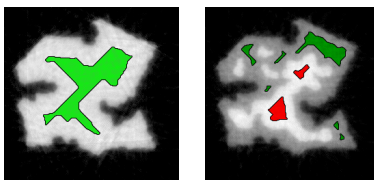


Figure 7: USP's of phantom image 4(a) and 4(c)

In practice, the USP will be *selected* by the user, based on the initial reconstruction. To avoid the subjectiveness of an actual user in the experimental results, the USPs for the experiments were automatically generated, using knowledge of the phantom. The USP for each grey level was computed by iteratively applying a binary erosion operation on the phantom region for that grey level, until a certain fraction of the pixels was left. The results are similar to a USP selection made by an actual user based on an initial grey level reconstruction, who selects a region that is well within the interior of the region for that grey level. In all experiments, the same USP was used to obtain the DGLS and MED results. For all grey level estimation procedures, the absolute difference with respect to the true grey level was computed. In case multiple grey levels had to be estimated (such as for phantom image 4(c) and 4(d)), the absolute differences were summed. For the family of phantom images in 4(d), we plotted the average absolute differences and their confidence intervals. The following series of experiments were run, varying only one parameter at a time:

- The **number of projections** from which the image was reconstructed was varied from 15 up to 180. In this experiment, the projections were

equiangularly selected in the interval $[0^\circ, 180^\circ]$. For each grey level, the USP contains 25% of the pixels for that grey level. Fig. 5(a) and 5(b) show reconstructions of phantom image 4(c) for 180 and 15 projection angles, respectively.

The results, plotted in Fig. 12, show that DGLS for both SIRT and SIRT-P generally yields much more accurate estimations than the MED estimations. Only when there are very few projection angles (e.g. 15), a significant error is visible. In phantom image 4(c) and 4(d), DGLS based on the unconstrained SIRT penalty function shows a large error when a small number of projection angles is used. We believe that this is related to the nonuniqueness issues of Prop. 1. In all subsequent experiments, only 30 projection angles were used as we can conclude that adding more projection angles does not improve the estimation accuracy by much.

- The **angular range** of the projections was varied from 180° down to 100° , from which 30 equiangular projections were selected. For each grey level, the USP contains 25% of the pixels for that grey level. Fig. 5(c) shows that reducing the angular range has a degrading effect on reconstructions, leading to artifacts. Fig. 13 shows that although the estimation error in absolute value is larger than in the previous experiment, the DGLS error is significantly lower than the error of the median value. The results for the family of phantoms, plotted in Fig. 13e, show that for both SIRT and SIRT-P, the corresponding DGLS variants yield far more accurate estimates than the respective MED results.
- The **noise level** of the projections was varied. In this experiment, Poisson noise was applied to the projection data, for a varying source intensity. By *number of counts per detector element*, we refer to the measured detector count when there is no object blocking the path from source to detector. The higher this count, the higher the Signal-to-Noise ratio. For the reconstruction, 30 projection angles were equally spaced in $[0^\circ, 180^\circ]$. For each grey level, the USP again contains 25% of the pixels for that grey level.

The effect of Poisson noise on a reconstruction is visible in Fig. 6. Fig. 14 shows that for the investigated noise range, the noise level does not have a major impact on the estimation error, for both the MED and DGLS estimates. This can be explained by the fact that only 30 projections are used, such that the reconstruction errors due to the small number of projections are much more significant than those related to the noise in the projection data.

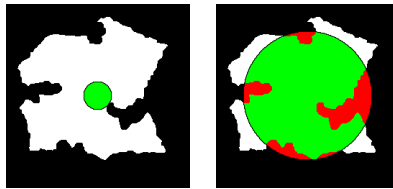
- The **size of the USP**, as a percentage of the total region for each grey level, was varied by iteratively applying an erosion filter as discussed above. Fig. 7 shows the user-selected part for phantom image 4(a) and 4(c), 20% the size of the original phantom. Fig. 15 shows that accurate grey level estimation is possible even if the USP is relatively small, down to 10% of the object size.

The results suggest that the DGLS method is robust with respect to the number of projection angles, the angular range, the level of noise and the size of the user-selected part. Moreover, DGLS typically yields a significantly more accurate estimate compared to computing the median value of the user-selected part. The results also demonstrate that more accurate estimation can be achieved by using the heuristic SIRT-P method as a scoring function instead of SIRT.

On our test PC, running at 2.4GHz, the running time of a single grey level estimation in all experiments but the first one was around 4 minutes. This is mostly attributed to the SIRT or SIRT-P algorithm that has to be performed every time while minimizing the grey level penalty function.

In all experiments described above, the USP for each grey level was selected as a proper subset of the actual regions in the phantom image. In practice, these regions must be selected by the user, based on an initial non-discrete reconstruction that may be inaccurate and difficult to interpret. If the user selects a region that partially corresponds to a different grey level, the DGLS approach may fail. To investigate this, we performed the following experiment for phantom image 4(a): the USP was selected as a circle of varying radius,

centered in a fixed point (see Fig. 8). The DGLS methods, based on SIRT and SIRT-P respectively, were then applied based on 30 projections, distributed equally between 0° and 180° . Fig. 9 shows the estimated grey level as a function of the radius of the circular region. It can be clearly observed that the grey level estimate becomes highly unreliable if part of the USP extends beyond the actual grey level region. Therefore, **proper selection of the USP is crucial to obtaining reliable grey level estimation.**



(a) radius = 20 pixels (b) radius = 90 pixels

Figure 8: Circular USP of two different sizes on phantom image 4(a). Green pixels in the USP are part of the object, red pixels are not.

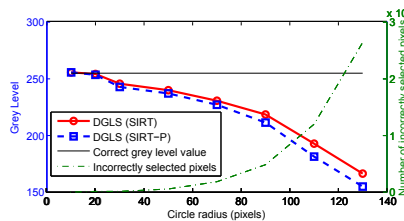


Figure 9: Grey level estimation using the proposed method when the USP is chosen too large.

4.2. Discrete tomography

The key motivation for the presented grey level estimation algorithm is that it allows for subsequent application of discrete tomography reconstruction algorithms. In this section, we will investigate how the reconstruction accuracy depends on the method used to estimate the grey level(s), for one particular discrete tomography algorithm called DART (Discrete Algebraic Reconstruction Technique). We remark that a full comparison between a range of proposed

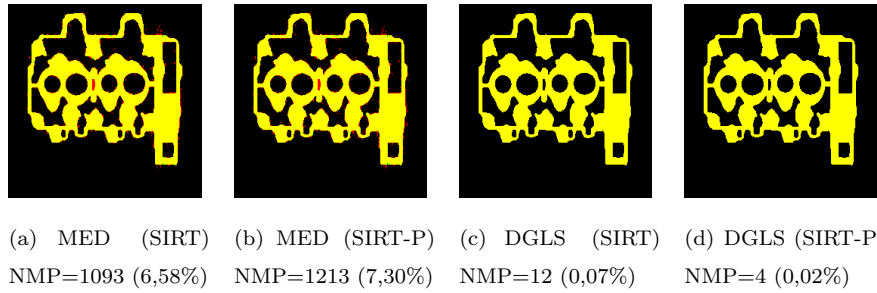


Figure 10: DART reconstructions of Phantom (b) with various grey level estimation methods.

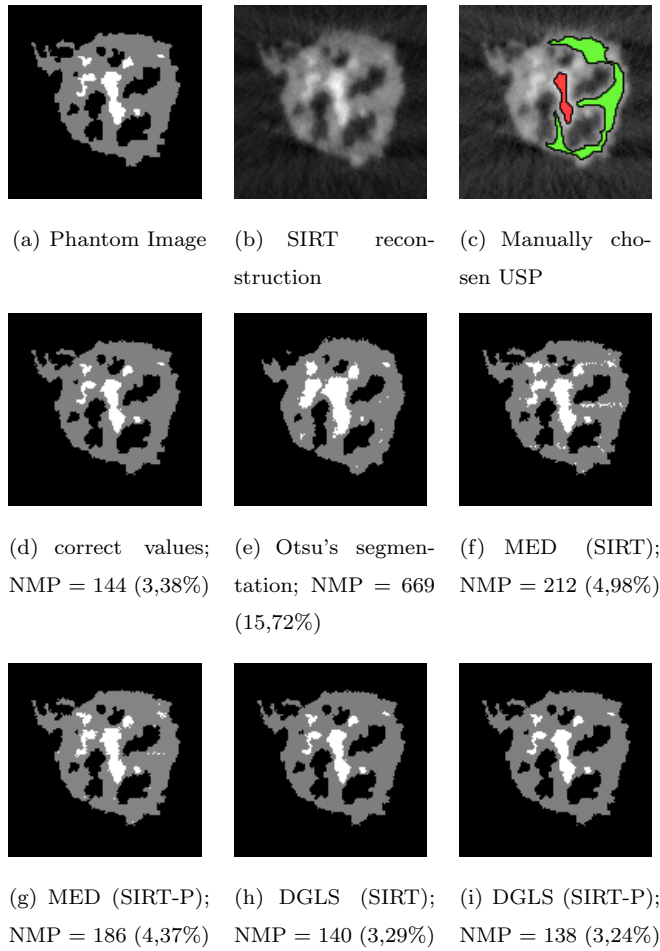


Figure 11: (f-i) DART reconstructions with various grey level estimation techniques.

discrete tomography algorithms would be a worthy subject for further investigation, yet we confine our experiments to a single algorithm to demonstrate the reconstruction accuracy that can be achieved by combining both methods (DGLS and DART).

Here, we briefly outline the DART algorithm. We refer to Batenburg and Sijbers [7], Batenburg et al. [8] for a more extensive description. DART is a heuristic algorithm that iterates between steps of an algebraic continuous reconstruction method, such as ART or SIRT, and discretization steps. In each DART iteration, the current reconstruction is segmented, after which the boundary of the segmentation regions is determined. Subsequently, one or more iterations of the continuous algebraic method are performed, while keeping the interior (i.e., non-boundary) pixels of the segmentation regions fixed at their known grey levels. Segmentation of the new reconstruction will result in a different boundary. Iterating this procedure leads to accurate discrete reconstructions in many cases, although convergence to a solution that satisfies the projection data cannot be guaranteed.

To evaluate the dependency of the reconstruction accuracy on the estimated grey levels, experiments were performed for phantom image 4(b), based on 30 noiseless projections, at equal angular intervals. After estimating the grey levels by either the MED or DGLS approach, a DART reconstruction was performed based on these grey levels, using SIRT as the underlying continuous algorithm. Fig. 10 shows the misclassified pixels in the DART reconstruction for the various estimation approaches, as well as for perfectly estimated grey levels (based on the phantom). The overlap between the phantom image and the reconstruction is coloured yellow. The differences are indicated in red (falsely reconstructed foreground pixel) and green (false background pixel) respectively. The total number of misclassified pixels is denoted by *NMP* in the figure captions.

As a second experiment, we performed a simulation of an electron tomography experiment, similar to the experiments reported in Batenburg et al. [8] (Section 5.2), using a phantom based on an experimental dataset of a bamboo-like carbone nanotube that was formed around a Copper catalyst particle. Fig.

11(a) represents a cross-section of the catalyst nanoparticle that contains both Copper (Cu, white) and Copper-Oxide (CuO, grey), as well as several voids. Projection data was simulated for an angular range of $-77,^\circ$ to $+77,^\circ$. Experimental instability in the alignment of the projections was simulated by shifting each projection by a random distance in the interval $[-1, +1]$, and Poisson noise was incorporated in the projection simulation. Fig. 11(b) shows the resulting SIRT reconstruction. To mimic a real experiment, the USP was selected manually, as shown in Fig. 11(c). Fig. 11(d) shows the reconstruction image of 11(b) segmented with the well-known Otsu’s segmentation method. The next five images show the segmented DART reconstructions based on perfect prior knowledge of the grey levels (e), MED (SIRT) (f), MED (SIRT-P) (g), DGLS (SIRT) (h) and DGLS (SIRT-P) (i). Although the difference between the DGLS and MED approaches is not as large as for the experiment based on phantom 4(b), the number of misclassified pixels for DGLS is very close (and even slightly better) to the value obtained using perfect prior knowledge, whereas the MED estimations result in significantly more misclassified pixels.

5. Discussion

The grey level estimation problem, when posed in its general form, does not guarantee a unique solution. The experimental results show that even for a moderately large number of 15 projections, additional constraints may be necessary to obtain an accurate estimate of the grey levels using our proposed approach. Several techniques can be used to improve the accuracy of the estimate:

- **Use a more accurate scoring function.** The projection distance, as computed using SIRT, does not incorporate nonnegativity constraints. Adding a nonnegativity heuristic to the reconstruction algorithm seems to result in improved accuracy of the grey level estimate, but its theoretical properties are hard to verify. A scoring function that incorporates both minimization of the projection distance and nonnegativity constraints (based on the nonnegative least squares problem) could result in

more accurate scoring, at the expense of long running times.

- **Simultaneous estimation of several grey levels.** In the approach presented in this paper, each of the grey levels is estimated independently. Simultaneous estimation of all grey levels, where the grey level in all user-selected parts is required to be constant, would provide more constraints for the estimation problem. However, this would also make the approach less robust, as an error in the choice of one USP will lead to errors all estimated grey levels.

Still, restricting the reconstruction outside the user-selected part to nonnegative values still does not capture the full set of available constraints. To incorporate the fact that the entire image should contain only a small, discrete set of grey levels, it seems necessary to actually attempt to *compute* such a discrete reconstruction for varying grey levels, and check which grey levels correspond to a consistent reconstruction. At present, the enormous computational requirements render this approach infeasible. We feel that estimation based on continuous methods using the DGLS approach, followed by a discrete reconstruction algorithm, results in a good trade-off between accuracy and speed. As demonstrated in Section 4.1, proper selection of the USP is crucial to the accuracy of the resulting DGLS estimate. The proposed approach still requires user interaction and leaves the possibility of user mistakes in the USP selection procedure. In future research, we aim at the development of algorithms for carrying out the USP selection task. A basic algorithm that is based on a rudimentary segmentation of the image may already be suitable for objects that are relatively simple, or for which a high quality reconstruction is already available. More complex objects will require more advanced algorithms that can change the USP depending on the scoring function.

6. Conclusions

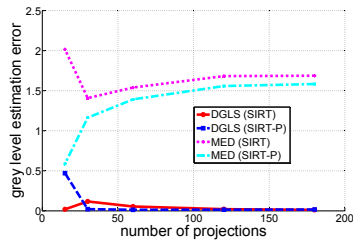
In this paper, we presented the DGLS approach: a semi-automatic method for estimating the grey levels of an unknown image from its projections. Grey

level estimation is a necessary step before applying discrete tomography algorithms, as these algorithms typically assume the set of admissible grey levels to be known a priori. In its general form, the grey level estimation problem does not guarantee a unique solution. To allow for reliable estimates, additional prior knowledge must be incorporated. In our semi-automatic approach, this prior knowledge is included by letting the user select a region that is known to correspond to a constant grey level, based on an initial non-discrete reconstruction.

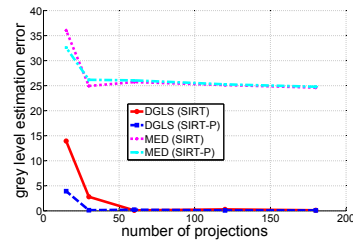
The proposed algorithm, which minimizes a penalty function while varying the grey level of the user-selected part, was shown to yield more accurate grey level estimates compared to direct estimation based on a continuous reconstruction. In particular, when a heuristic is used to enforce positivity of the image reconstructed during the penalty computation, accurate estimates can be obtained even from a small number of projection images, or a small angular range. An important question that remains for future research, is to determine what accuracy is actually required for the estimation step to use discrete tomography effectively.

- [1] G. T. Herman and A. Kuba, editors. *Discrete Tomography: Foundations, Algorithms and Applications*. Birkhäuser, Boston, 1999.
- [2] G. T. Herman and A. Kuba, editors. *Advances in Discrete Tomography and its Applications*. Birkhäuser, Boston, 2007.
- [3] T. Schüle, C. Schnörr, S. Weber, and J. Hornegger. Discrete tomography by convex-concave regularization and d.c. programming. *Discr. Appl. Math.*, 151:229–243, 2005.
- [4] K. J. Batenburg. A network flow algorithm for reconstructing binary images from continuous X-rays. *J. Math. Im. Vision*, 30(3):231–248, 2008.
- [5] H. Y. Liao and G. T. Herman. A coordinate ascent approach to tomographic reconstruction of label images from a few projections. *Discr. Appl. Math.*, 151:184–197, 2005.

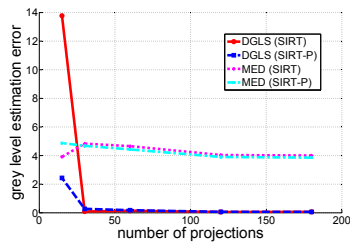
- [6] A. Alpers, H. F. Poulsen, E. Knudsen, and G. T. Herman. A discrete tomography algorithm for improving the quality of 3DXRD grain maps. *J. Appl. Crystall.*, 39:582–588, 2006.
- [7] K. J. Batenburg and J. Sijbers. DART: A fast heuristic algebraic reconstruction algorithm for discrete tomography. In *Proc. of the IEEE Int. Conf. on Image Proc. (ICIP)*, pages IV 133 – IV 136, 2007.
- [8] K. J. Batenburg, S. Bals, J. Sijbers, C. Kübel, P.A. Midgley, J.C. Hernandez, U. Kaisere, E.R. Encina, E.A. Coronado, and G. Van Tendeloo. 3D imaging of nanomaterials by discrete tomography. *Ultramicroscopy*, 109: 730–740, 2009.
- [9] S. Bals, K. J. Batenburg, J. Verbeeck, J. Sijbers, and G. Van Tendeloo. Quantitative 3D reconstruction of catalyst particles for bamboo-like carbon-nanotubes. *Nano Letters*, 7(12):3669–3674, 2007.
- [10] S. Bals, K. J. Batenburg, D. Liang, O. Lebedev, G. Van Tendeloo, A. Aerts, J. A. Martens, and C. E. A. Kirschhock. Quantitative three-dimensional modeling of Zeotile through discrete electron tomography. *J. Am. Chem. Soc.*, 131(13):4769–4773, 2009.
- [11] P. Gilbert. Iterative methods for the three-dimensional reconstruction of an object from projections. *J. Theoret. Biol.*, 36:105–117, 1972.
- [12] J. Gregor and T. Benson. Computational analysis and improvement of SIRT. *IEEE Trans. Medical Imaging*, 27(7):918–924, 2008.
- [13] R. P. Brent. *Algorithms for minimization without derivatives*. Prentice-Hall, Englewood Cliffs, New Jersey, 1973.



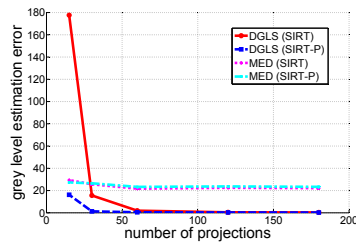
(a) Phantom a



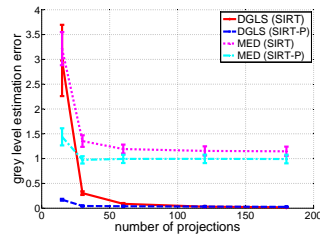
(b) Phantom b



(c) Phantom c



(d) Phantom d



(e) Phantom e

Figure 12: Error of grey level estimation with varying numbers of projection angles.

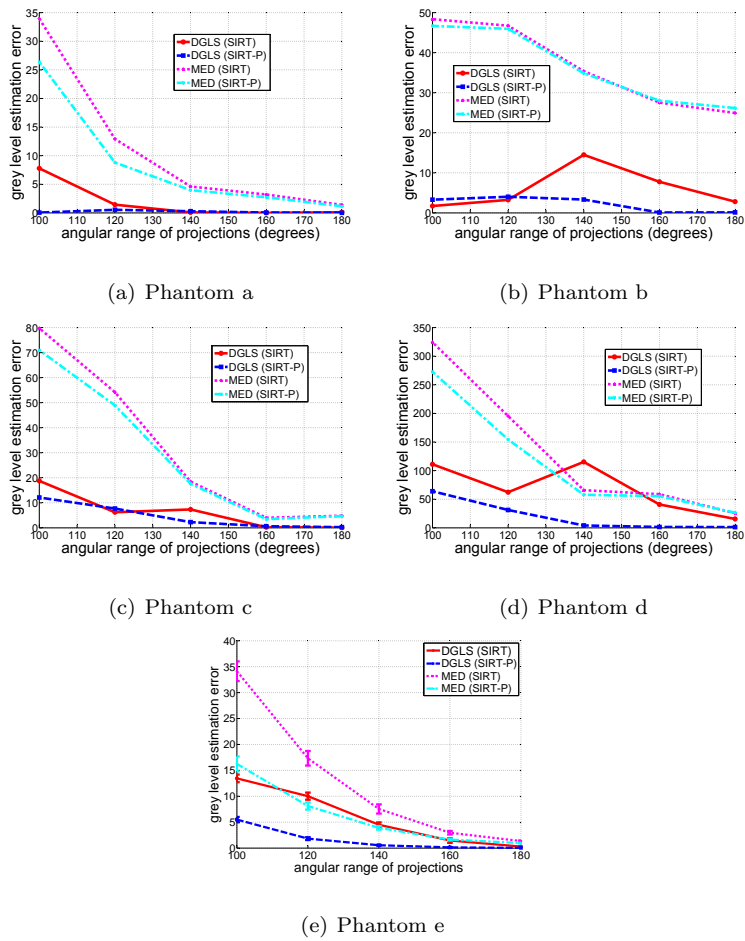
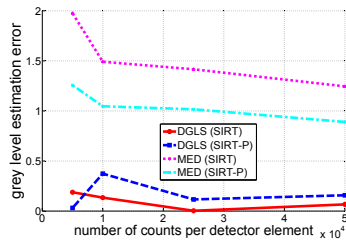
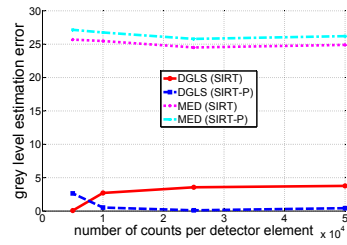


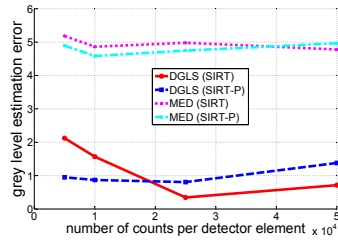
Figure 13: Error of grey level estimation with varying ranges of projection angles.



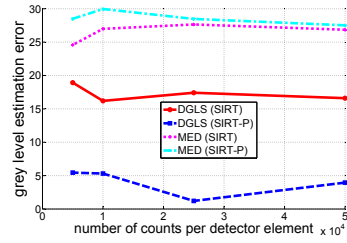
(a) Phantom a



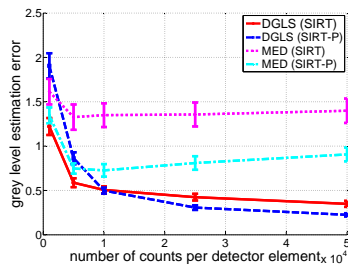
(b) Phantom b



(c) Phantom c



(d) Phantom d



(e) Phantom e

Figure 14: Error of grey level estimation with different noise levels.

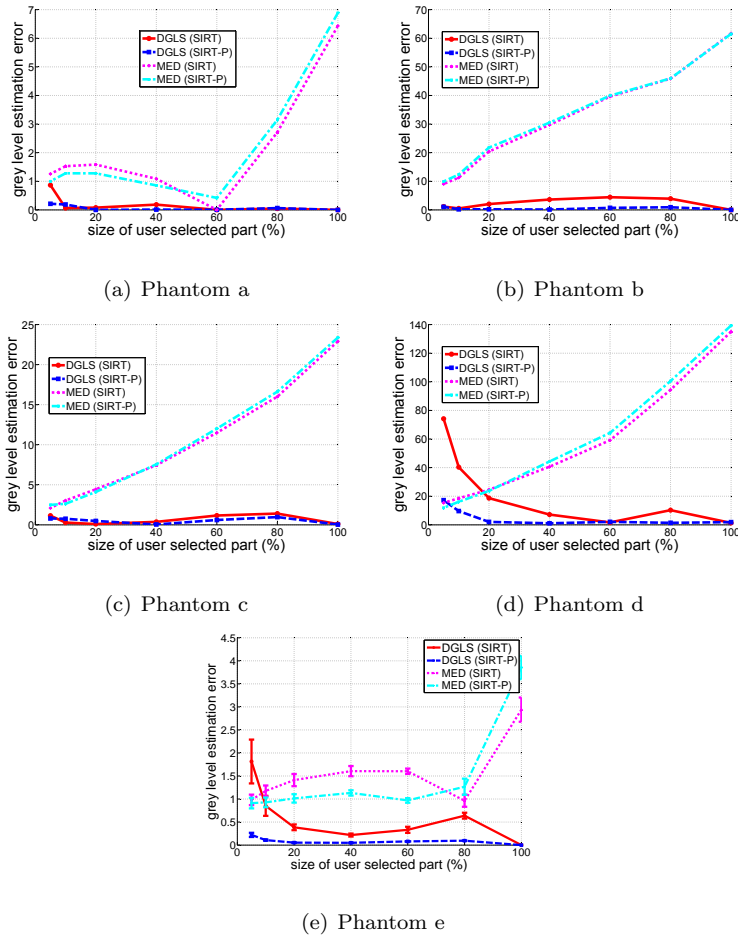


Figure 15: Error of grey level estimation with different sizes of the user-selected part.